ACS APPLIED MATERIALS & INTERFACES

Research Article

www.acsami.org

Paper-Based Microfluidics: Fabrication Technique and Dynamics of Capillary-Driven Surface Flow

Joel Songok,*[,†] Mikko Tuominen,[‡] Hannu Teisala,[‡] Janne Haapanen,[§] Jyrki Mäkelä,[§] Jurkka Kuusipalo,[‡] and Martti Toivakka[†]

[†]Laboratory of Paper Coating and Converting and Center for Functional Materials, Abo Akademi University, Porthaninkatu 3, 20500 Åbo/Turku, Finland

[‡]Paper Converting and Packaging Technology, Department of Materials Science and [§]Aerosol Physics Laboratory, Department of Physics, Tampere University of Technology,33101 Tampere, Finland

Supporting Information

ABSTRACT: Paper-based devices provide an alternative technology for simple, low-cost, portable, and disposable diagnostic tools for many applications, including clinical diagnosis, food quality control, and environmental monitoring. In this study we report a two-step fabrication process for creating two-dimensional microfluidic channels to move liquids on a hydrophobized paper surface. A highly hydrophobic surface was created on paper by TiO_2 nanoparticle coating using a high-speed, roll-to-roll liquid flame spray technique. The hydrophilic pattern was then generated by UV irradiation through a photomask utilizing the photocatalytic property of TiO_2. The flow dynamics of five model liquids with differing surface tensions 48−72 $mN{\cdot}m^{-1}$ and viscosities 1−15 $mN{\cdot}m^{-2}$ was studied. The results show that the liquid front (l) in a channel advances in time (t) according to the power law $l = Zt^{0.5}$ (Z is an empirical constant which depend on the liquid properties and channel dimensions). The flow dynamics of the liquids with low viscosity show a dependence on the channel width and the droplet volume, while the flow of liquids with high viscosity is mainly controlled by the viscous forces.

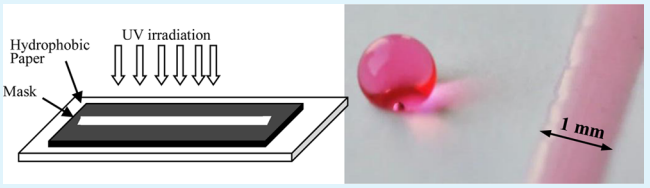

KEYWORDS: *paper-based microfluidics, capillary flow, surface wettability control, two-dimensional lateral flow*

INTRODUCTION

Conventional uses of paper are in applications such as writing, printing, cleaning, food wrapping, filtering, packaging, and as currency. In recent times, paper has become increasingly recognized as an interesting substrate for the construction of (paper-based) microfluidic devices (μPADs) for possible applications in areas such as environmental monitoring, health diagnosis, food safety, and for home-care. Paper offers numerous advantages, including low cost, ease of handling and disposal, hydrophilicity-driven flow eliminating the need for pumps or power, and removal of problems associated with bubbles.[1−4] μPADs are constructed both for detection and delivery of a sufficient volume of fluid from a sample well to a sensing zone. However, commonly more than 50% of the sample is retained within the paper matrix.[5] To make a μPAD, it is necessary to design paper with hydrophilic regions, that is, channels that wick fluids, bounded by regions of hydrophobic walls[6] or air.[7,8]

A number of patterning methods for μPADs have been proposed in literature, including the following: photolithography,[3,9−12] inkjet etching,[13−15] plasma etching,[16,17] polydimethysiloxane (PDMS) plotting,[18] PDMS printing,[19] knife cutting,[7] laser cutting,[8,20] and wax printing[21−24] and dipping.[25] Comprehensive and comparative information on these methods can be found in recently published review articles.[5,26−28] Although each fabrication technique has its advantages and shortcomings, the need still remains for simple fabrication techniques that can produce μPADs in large volumes with high reproducibility and low cost. In addition, the devices should efficiently deliver maximal liquid volumes to the detection zone.

This article describes a two-step method for fabricating two-dimensional (2D) microfluidic channels by controlling the local wettability of paper surface. The use of surface wettability control for paper microfluidic applications has been reported earlier. Balu et al. (2009) made 2D paper-based μPADs by printing high surface energy black ink patterns on paper substrates. The ink patterns provided local handling of droplet adhesion on the paper surface and hence enabled storage, transport, mixing, sampling, and splitting of droplets of test liquids on the surface.[29] Barona and Amirfazli (2011) prepared superhydrophobic paper based on spraying a nanocomposite film and further manipulated the wetting characteristics of the paper by printing solid gray patterns of different intensities with a simple printing technology.[30] In the current study, the photocatalytic property of titanium dioxide is utilized to

Received: August 21, 2014
Accepted: October 22, 2014
Published: October 22, 2014

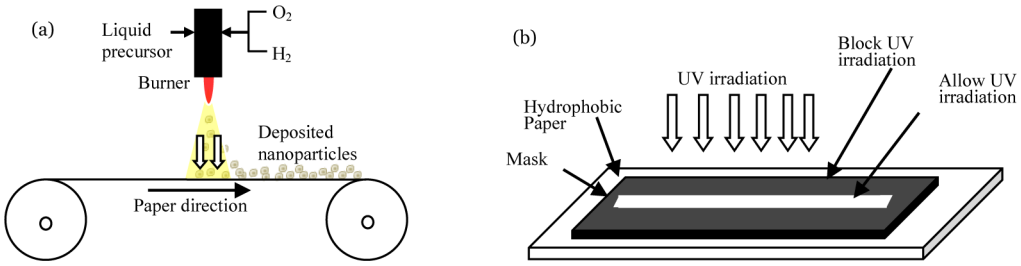

Figure 1. A schematic for manufacturing of paper-based microfluidic channels. (a) Generation of a hydrophobic paper surface by TiO_2 nanoparticle deposition in the roll-to-roll LFS process. (b) Creation of hydrophilic surface flow channels by UV irradiation through a mask.

generate wettability contrast. A thin, transparent, and highly hydrophobic surface layer was created by coating nanosized TiO_2 particles on paper surface using the liquid flame spray (LFS) technique. The LFS is a thermal technique for generating and coating surfaces with metal oxide nanoparticles.[31,32] Hydrophilic channels were then generated by UV irradiation through a photomask placed on the TiO_2-coated paper. The unexposed regions retain their superhydrophobicity, thereby acting as a boundary for the open microfluidic channels capable of transferring liquids via capillary action. This technique is valuable for the following reasons: the deposition of TiO_2 nanoparticles on paper can be accomplished in a roll-to-roll process, which enables continuous high-speed and large volume industrial production. Second, by controlling the paper surface wettability, liquid flow over the surface is enhanced, which minimizes liquid absorption into paper and reduces the required sample volumes. Finally, the liquid flow speeds can be controlled by adjusting the apparent surface energy in the channels with the amount of UV exposure.

This paper describes a novel way of producing channels for lateral flow microfluidic applications. We optimize the UV irradiation time and demonstrate the potential of the fabrication technique for paper-based microfluidics by investigating the influence of channel width, droplet volume, and liquid properties on the rate of liquid flow for five model liquids.

MATERIALS AND METHODS

Figure 1 below presents a schematic for creating a paper-based microfluidic channel. First, a commercially available pigment-coated paperboard (200 g/m^2, Stora Enso, Sweden) was coated with TiO_2 nanoparticles in a continuous roll-to-roll process using the LFS method. The LFS coating was carried out in the pilot scale paper converting line at Tampere University of Technology (TUT). A detailed description of the LFS process has been presented previously.[33,34] Here, channels that were 0.5, 1.0, and 1.5 mm in width and 60 mm in length were studied. The hydrophilic channels were created by ultraviolet (UVA − 320−390 nm) exposure (Bluepoint 4 ecocure, Hönle UV technology, DE) through a photomask. Different irradiation times, 2, 10, 15, and 30 min, were used to understand the induced changes in paper wettability and optimize the exposure time. The photomask was created by printing silver nanoparticle ink (Sun Tronic U5603, Suntronic Inc., US) onto a microscopic glass slide (Thermo-Scientific, Menzel-gläzer GmbH, DE) using an inkjet printer (DimatixTM materials printer DMP-2831, Fujifilm, US). The measured widths of the channels after UV irradiation were ca. 5% narrower than the width defined by the mask. The surface wettability was characterized by contact angle measurements (KSV CAM 200, KSV Instruments Ltd., FI) using a Laplacian fit to the projected 4 μL droplet curvature.

The flow dynamics within the channels were investigated using the setup shown in Figure 2. The sample to be tested was placed on a horizontal x−y stage, and a liquid droplet was deposited on one end of

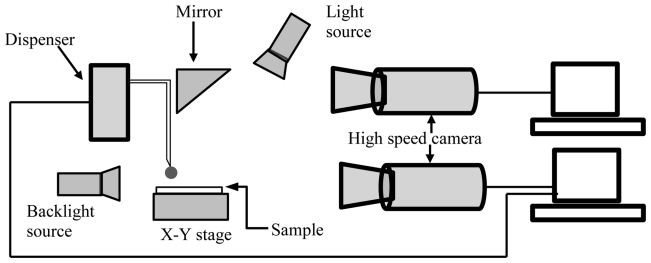

Figure 2. Experimental setup with two cameras for recording side and top views of liquid flow on microchannels on paper.

the channel using the dispenser of the KSV CAM 200 equipment. The position of the liquid front over time was recorded using two cameras: one from a side view recording 100 frames per second and one from a top view recording at 200 frames per second. A small amount of amaranth red dye was added to the liquids to improve the visual contrast of the thin liquid films. The results are presented as averages of 4−6 parallel measurements. The distance of the advancing wetting front as a function of time was measured from the recorded frames using ImageJ image analysis software.[35] Table 1 lists the physical properties of the liquids used in this study. PhysicaMCR 300 rheometer (Anto Paar GmbH, AT) was used to measure liquid viscosity and the Sensadyne bubble tensiometer (M&H Technologies Inc., US) for surface tension measurements. The measured values are comparable to what is available in literature. All the measurements were conducted at ambient conditions at room temperature.

RESULTS AND DISCUSSION

Wettability Control. Figure 3 below shows liquid placed on wetting and nonwetting regions of the paper used in this work. The hydrophilic channel on the otherwise hydrophobic paper surface was created by exposing the TiO_2 nanoparticle-coated paper to UV irradiation through a patterned photomask.

Contact angle (CA) measurements show that the TiO_2 nanoparticle coating by the LFS technique changed the wettability of the paperboard from slightly hydrophilic (CA ≈ 80°) to superhydrophobic (CA ≈ 150°, step 1, Figure 4). The superhydrophobicity has been attributed to a combination of the nanoparticle surface chemistry and the hierarchical surface roughness that enhances the water repellency.[34,36] By exposing the TiO_2-coated paper to UV irradiation (wavelength 320−390 nm), the superhydrophobic surface is converted to a superhydrophilic one with a contact angle ≤ 10°, (step 2, Figure 4). The conversion has been ascribed to an increase in the number of hydroxyl groups caused by photocatalytic oxidation of the thin carbonaceous layer covering the TiO_2 nanoparticles.[32,36−38] Tuominen et al. (2014) has reported a superhydrophobic−hydrophilic conversion in a roll-to-roll process with line speeds up to 10 m/min using corona and argon plasma treatment.[39] The wettability conversion to a water

dx.doi.org/10.1021/am5055806 | ACS Appl. Mater. Interfaces 2014, 6, 20060−20066

Table 1. Physical Properties of the Tested Liquids

liquid	abbreviation	density (kg m^{-3})	viscosity (mPa·s)	surface tension (mN/m)	bond number (1 μL droplet)	bond number (8 μL droplet)
deionized water	ST72_V1.0	1000	1.0	72	0.05	0.21
5% v/v isopropanol–water	ST54_V1.5	989	1.5	54	0.07	0.28
10% v/v isopropanol–water	ST48_V1.7	978	1.7	48	0.08	0.31
50% v/v glycerol–water	ST66_V8.5	1144	8.5	66	0.07	0.26
62% v/v glycerol–water	ST64_V15.5	1174	15.5	64	0.07	0.28

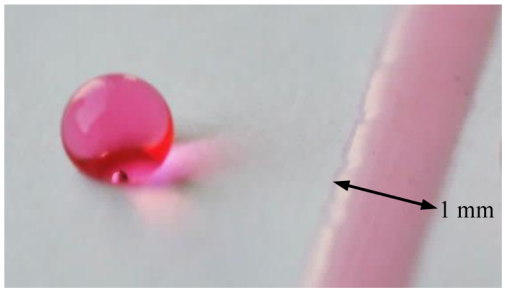

Figure 3. A water droplet deposited on TiO_2 nanoparticle-coated paper and a 2D microfluidic channel confined within a superhydrophobic boundary.

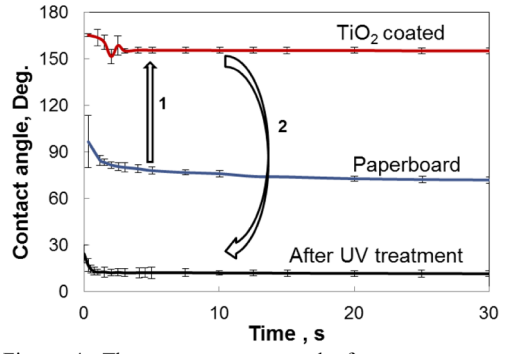

Figure 4. Water contact angle for a paper sample as a function of time: paperboard before coating with TiO_2 nanoparticles (blue line), after TiO_2 coating (red line), and after subsequent exposure to UV light (black line).

contact angle of ~20° was achieved within 0.8 s when corona treated at 8 m/min line speed and within 0.2 s applying plasma treatment at line speed of 12 m/min. The fairly constant static contact angle implies a low or no liquid absorption into paper over the 30 s time observed herein. This is an advantage since if the liquid transport takes place on the paper surface with no absorption into the paper matrix, sample volumes available for lateral flow transfer are maximized.

Influence of Irradiation Time. The conversion from a superhydrophobic to highly hydrophilic surface depends on the irradiation intensity and irradiation time. In the current work, constant irradiation intensity of 50 mW/cm^2 was used in laboratory scale. High-intensity industrial light-emitting diode and pulsed UV systems can be used to significantly reduce the required exposure times, potentially enabling roll-to-roll exposure through a photomask. Figure 5 presents the contact angles at 2, 10, and 20 s after the droplet deposition on paper treated with different irradiation times. UV irradiation altered the deionized water and 62% v/v glycerol–water mixture contact angles. The contact angles decrease with increasing UV irradiation time to the 10 min exposure. Shorter irradiation times lead to intermediate contact angles that can potentially be advantageous in controlling and manipulating flow rates and may also be used to create reaction sites. The slightly higher contact angles for the glycerol–water mixture at 2 s after the droplet placement on the sample is from the high viscosity slowing the contact angle while it approaches its static value. Because of differences in liquid properties used and to eliminate the possibilities of partial wettability conversion, the samples in this work were exposed to UV irradiation for 30 min.

Flow Dynamics in 2D Microchannel. One of the advantages of using paper as a substrate for microfluidic devices is its ability to transport liquid by capillary action. When a liquid droplet is placed on a hydrophilic 2D microchannel created by the UV exposure, it spreads spontaneously as shown in Figure 6. The liquid is confined to the hydrophilic area and does not spread onto the hydrophobic regions. (See also Supporting Information for videos of different liquid flows that were used to plot the position of the advancing wetting front as a function of time presented in Figure 7.)

Figure 7 summarizes the data for the five test liquids flowing on a 1.5 mm wide channel. These data are presented in terms

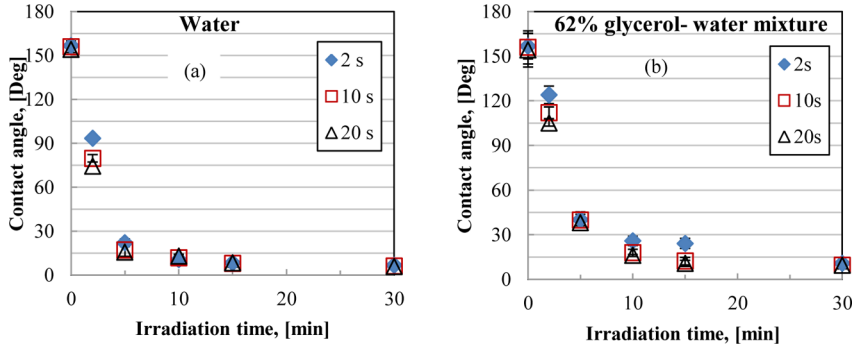

Figure 5. Water (a) and 62% glycerol–water mixture (b) contact angles at different UV irradiation times. For each irradiation time, the angle was recorded after, 2, 10, and 20 s after the droplet was deposited on the surface.

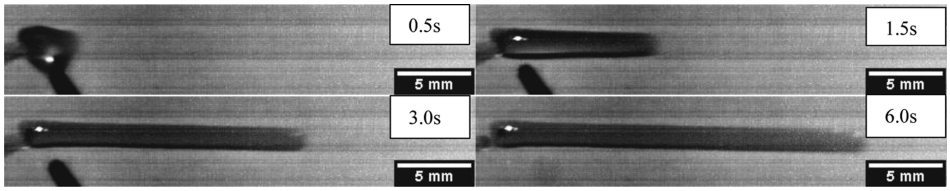

Figure 6. Images of 50% v/v glycerol–water mixture advancing in a 2D microchannel.

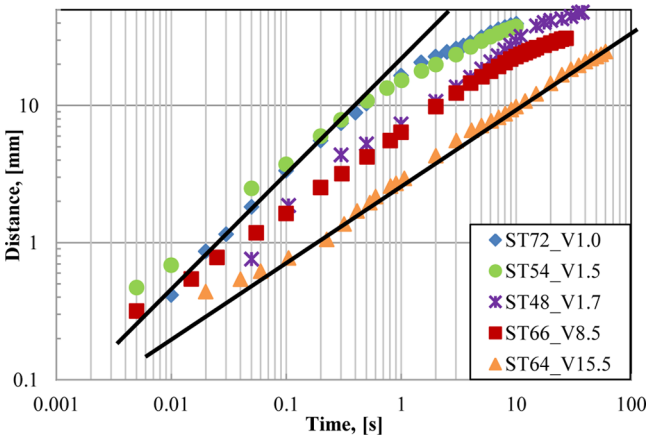

Figure 7. Spreading kinetics of different liquids on a 1.5 mm channel. Droplet volume = 8 μL.

of advancing liquid front position versus time. As expected, low-viscosity liquids have fastest spreading rates. For a high viscosity liquid (e.g., ST64_V15.5), a single flow regime is observed implying the wetting force-driven flow is controlled by viscous forces at all times. In the case of a low-viscosity liquid (e.g.ST72_V1), two flow regimes can be seen. Initially, the flow is influenced by the relaxation of the advancing contact angle toward its static equilibrium value. At longer times, a second regime emerges from the balance between surface tension and viscous forces close to the contact line. The inertial effects can be considered negligible because both the Reynolds number and Weber number are low for the studied system. The significance of the gravitational force relative to capillary forces can be expressed using the Bond number (Bo):

$$\mathrm{Bo} = \rho\gamma R^2/g$$

where g is the gravitational acceleration, R is the radius of the spherical droplet before spreading, and ρ and γ are the liquid density and surface tension, respectively.[40] The Bo ranges between 0.06 and 0.31 for the liquids used in this study (Table 1). Since the Bo < 1, the gravitation effect was considered negligible.

The extent of wetting versus the square root of time plots is presented in Figure 8. The experimental data are fitted to the power law of the form

$$l = Zt^n$$

where l is the spreading distance, t is time, and Z and n are empirical constants determined by the best fit of each curve. The fits with $R^2 > 0.98$ indicate that the liquid front advances approximately proportionally to square root of time ($l \sim \sqrt{t}$). The curves for the less-viscous liquids (ST72_V1.0 and ST54_V1.5) were fitted to the point where the flow rate starts to decrease due to insufficient liquid supply to the liquid front.

Figure 9 shows the values of empirical constants n and Z obtained for different channel width and droplet volume combinations. Despite the major difference in the velocity profiles and the presence of the deformable free surface on open channels, the same $t^{0.5}$ time dependence is observed for a closed capillary,[41] a surface groove capillary,[42] and the 2D open lateral flow channel of the current work. The $t^{0.5}$ behavior may reflect a constant pressure difference driving the flow as liquid moves on the channel. The value of n was found to be independent of the liquid property, channel width, and the liquid volume. However, the flow was strongly influenced by prefactor Z, which shows dependence on the liquid properties, droplet volume, and the channel width. Figure 9 shows that the viscous liquid (ST64_V15.5) is not adversely affected by changes in the droplet volume and channel width, which confirms the viscous dominance for the flow. On the contrary, for the less-viscous liquids (ST72_V1.0, ST54_V1.5, and ST48_V1.7), an increase in the channel width and the droplet volume results in a significant change in the Z value except for 8 μL water droplet on 1 mm channel that showed no flow. We

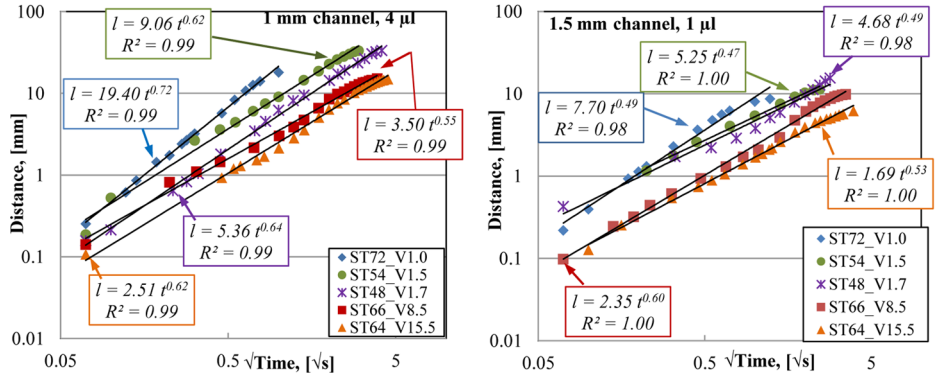

Figure 8. Dependence of the spreading distance over $\sqrt{t}$. All the measurements indicate a power law behavior with $R^2 > 0.98$. Continuous lines show power law fits.

dx.doi.org/10.1021/am5055806 | ACS Appl. Mater. Interfaces 2014, 6, 20060–20066

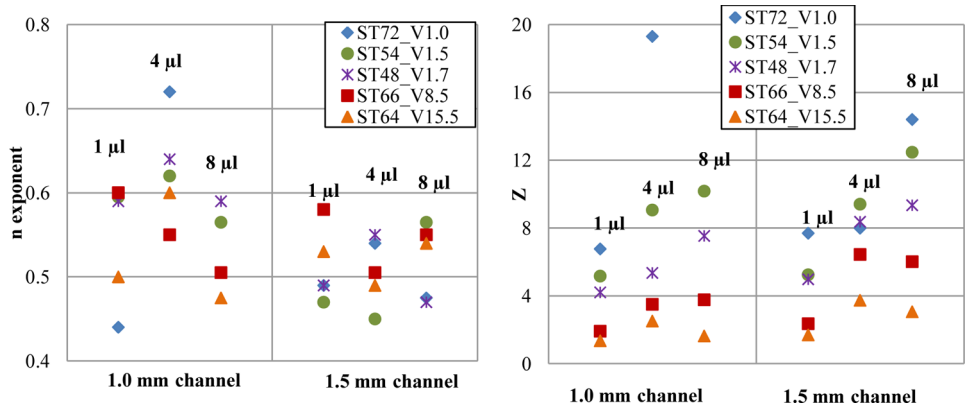

Figure 9. Power law constants *n* exponent (left) and prefactor *Z* (right) obtained from best fits for flows on 1 mm and 1.5 mm channels.

concluded that nonflow is due to resistance offered by small channel in addition to the high liquid surface tension.

Influence of the Liquid Surface Tension and Channel Width. The positions of the spreading fronts for different liquids advancing on 1.0 and 1.5 mm wide channels at 1, 2, 3, and 10 s are compared in Figure 10. After 10 s, the spreading of

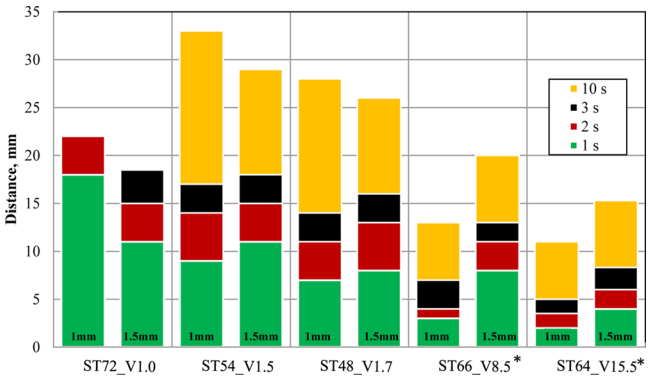

Figure 10. Effect of liquid properties on the position of the advancing liquid front on 1.0 and 1.5 mm wide channels for a droplet volume of 4 μL. *Liquid front continues spreading beyond 10 s.

the less-viscous liquids (ST72_V1.0, ST54_1.5, and ST48_V1.7) was complete. These times are of interest because the majority of microfluidic applications requiring fast analysis are conducted within this time frame. Second, liquid absorption into paper is minimal at these times (as shown in Figure 4), and evaporation may be considered negligible.

Comparing the liquid front position for the different liquids in Figure 10, we can observe that low surface tension liquids (isopropanol–water mixtures) advanced the furthest. The main effect of the isopropanol addition is lowering the surface tension of water, which also lowers the contact angle and thereby determines the maximum extent of liquid spreading. Figure 10 further reveals that the water stops from advancing after 2 and 3 s on 1 and 1.5 mm channels, respectively. This appears to be related to the high surface tension of water, which confirms its controlling role on the flow. When comparing the two channel widths, the wider channel shows initially a higher flow rate within the first 3 s. This is attributed to the area available for the liquid to wet as it lowers Gibbs energy to an equilibrium state and also the higher resistance to flow on the narrow channel. However, at long times, the liquid front advances furthest in the narrow channel because more liquid is available to fill the channel.

When optimizing the liquid transfer rate and the volume, the channel width and the droplet size play important roles. A small droplet deposited on a wide channel resulted in short transport distances because of an insufficient volume of liquid available for spreading. Short distances were also seen when a large droplet was deposited on a narrow channel. In this case, the droplet formed a bulge shape, and the contact base diameter extended beyond the channel width, giving rise to an insufficient driving force to break the cohesive forces within the liquid. Figure 11 presents the dependence of the spreading

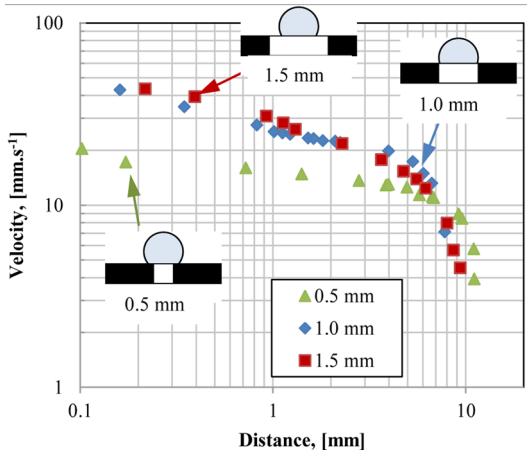

Figure 11. Dependence of the spreading velocity on the distance of the advancing liquid front. (insets) Illustrations of the different droplet morphologies on the hydrophilic channels.

velocity on the distance for 0.5 and 1.0 mm wide channels. We infer that the difference in velocities despite the small droplet size (1.24 mm diameter) is due to different droplet morphologies formed when droplets are deposited onto the channel. This is evident in Figure 12, which illustrates the shapes of the droplet formed as the water front advances on 0.5 and 1.0 mm wide channels. The bulge shape formed in 0.5 mm channels acts as a liquid source to the channel. This leads to a constant liquid front velocity along the channel as observed in Figure 11. For the wide channel, the water droplet just covers the hydrophilic area, leveling out evenly along the channel as the liquid front advances.

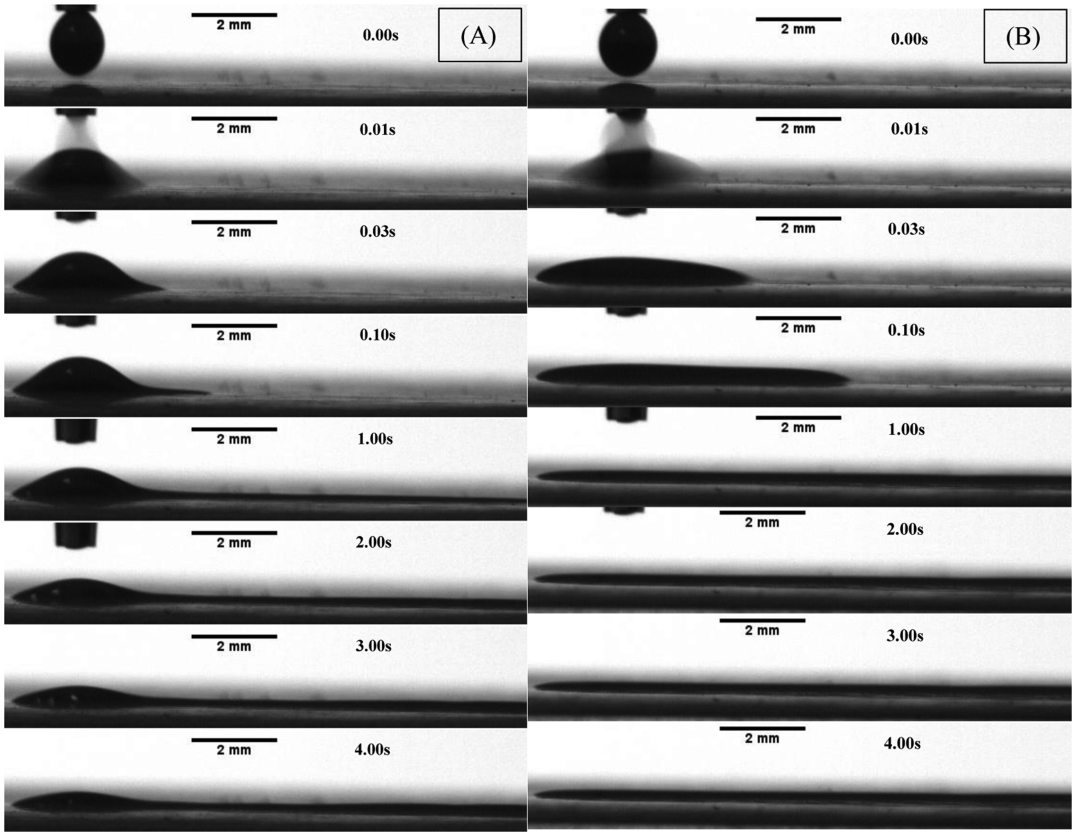

Figure 12. A side view of drop morphologies formed as liquid flows on the channel. A 1 μL water droplet (A) on 0.5 mm channel and (B) on 1.0 mm channel.

CONCLUSIONS

Photocatalytic property of TiO_2 was used to create hydrophilic–hydrophobic regions on paper surface. The two-step patterning process entailed coating paper with TiO_2 nanoparticles in a roll-to-roll process followed by a second step, in which the coated paper is exposed to UV light through a photomask. This enables fabrication of 2D microchannels with arbitrary geometry for control of lateral liquid flow on paper with minimal absorption into the paper matrix. Small volumes of different liquids with a surface tension range of 48–72 mN·m^{-1} and a viscosity range of 1–15 mN·m^{-2} flow within the channels driven by capillary action. From the range of liquid properties tested, other liquids within this property range such as bodily fluids and contamination in water can potentially be conveyed over distances of 20 mm within 2 s. For example, blood plasma, which is a Newtonian fluid with surface tension of 56 mN·m^{-1} and viscosity of 1.2 mPa.s,[43,44] may show similar flow rates as the sample ST54_V1.5, and urine from a human suffering with gall bladder stone having surface tension of 67 mN·m^{-1} and viscosity 8.5 mPa.s may exhibit flow rates comparable to the sample ST66_V8.5.[45]

ASSOCIATED CONTENT

Supporting Information

These videos, recorded from the top view at 200 frames per second, show the positions of the wetting fronts for the different liquids investigated. Additionally, a side-view video, recorded at 100 fps, shows water droplet deposition on a channel. This material is available free of charge via the Internet at http://pubs.acs.org.

AUTHOR INFORMATION

Corresponding Author

*Phone: +358 2 215 4232. E-mail: joel.songok@abo.fi.

Notes

The authors declare no competing financial interest.

REFERENCES

(1) Osborn, J.; Lutz, B.; Fu, E.; Kaumann, P.; Stevens, D. Y.; Yager, P. Microfluidics without Pumps: Reinventing the T-Sensor and H-Filter in Paper Network. *Lab Chip* **2010**, *10*, 2659–2665.

(2) Macek, K.; Bacvarova, H. Paper, Ready for Use Plates, and Flexible Sheets for Chromatography. *Chromatogr. Rev.* **1971**, *15*, 1–28.

(3) Martinez, A. W.; Phillips, S. T.; Carrilho, E.; Thomas, S. W., III; Sindi, H.; Whitesides, G. M. Simple Telemedicine for Developing Regions: Camera Phones and Paper-Based Microfluidic Devices for Real-time, Off-site Diagnosis. *Anal. Chem.* **2008**, *80*, 3699–3707.

(4) Yager, P.; Edwards, T.; Fu, E.; Helton, K.; Nelson, K.; Tam, M. R.; Weigl, B. H. Microfluidic Diagnostic Technologies for Global Public Health. *Nature* **2006**, *442*, 412–418.

(5) Li, X.; Ballerini, R.; Shen, W. A Perspective on Paper-Based Microfluidics: Current Status and Future Trends. *Biomicrofluidics* **2012**, *6*, 1–13.

(6) Stock, R.; Rice, C. F. B. In *Chromatographics Methods;* John Wiley & Sons: New York, 1974.

(7) Fenton, E. M.; Mascarenas, M. R.; López, G. P.; Sibbett, S. S. Multiplex Lateral-Flow Test Strips Fabricated by Two-dimensional Shaping. *ACS Appl. Mater. Interfaces* **2009**, *1*, 124–129.

(8) Nie, J.; Liang, Y.; Zhang, Y.; Le, S.; Li, D.; Zhang, S. One-Step Patterning of Hollow Microstructures in Paper by Laser Cutting to Create Microfluidic Analytical Devices. *Analyst* **2013**, *138*, 671–676.

(9) Martinez, A. W.; Phillips, S. T.; Butte, M. J.; Whitesides, G. M. Patterned Paper as a Platform for Inexpensive, Low-Volume, Portable Bioassays. *Angew. Chem., Int. Ed.* **2007**, *46*, 1318–1320.

(10) Martinez, A. W.; Phillips, S. T.; Wiley, B. J.; Gupta, M.; Whitesides, G. M. FLASH: A Rapid Method for Prototyping Paper-Based Microfluidics Devices. *Lab Chip* **2008**, *8*, 2146−2150.
(11) Nie, Z.; Nijhuis, C.; Gong, J.; Chen, X.; Kumachev, A.; Martinez, A. W.; Narovlyansky, M.; Whitesides, G. M. Electrochemical Sensing in Paper-Based Microfluidic Devices. *Lab Chip* **2010**, *10*, 477−483.
(12) Apilux, A.; Dungchai, W.; Siangproh, W.; Praphairaksit, N.; Henry, C. S.; Chailapakul, O. Lab-on-Paper with Dual Electrochemical/Colorimetric Detection for Simultaneous Detection of Gold and Iron. *Anal. Chem.* **2010**, *82*, 1727−1732.
(13) Abe, K.; Suzuki, K.; Citterio, D. Inkjet-printed Microfluidic Multi-Analyte Chemical Sensing Paper. *Anal. Chem.* **2008**, *80*, 6928−6934.
(14) Abe, K.; Kotera, K.; Suzuki, K.; Citterio, D. Inkjet-Printed Paperfluidic Immuno-Chemical Sensing Device. *Anal. Bioanal. Chem.* **2010**, *398*, 885−893.
(15) Maejima, K.; Expósito, B. G.; Suzuki, K.; Citterio, D. In All-Inkjet-Printed Microfluidic Paper-Based Analytical Devices; *8th International Paper and Coating Chemistry Symposium;* Innventia AB: Stockholm, Sweden, 2012; pp 282−285.
(16) Li, X.; Tian, J.; Garnier, G.; Shen, W. Fabrication of Paper-Based Microfluidic Sensors by Printing. *Colloids Surf., B* **2010**, *76*, 564−570.
(17) Li, X.; Tian, J.; Nguyen, N. T.; Shen, W. Paper-Based Microfluidic Devices by Plasma Treatment. *Anal. Chem.* **2008**, *80*, 9131−9134.
(18) Bruzewicz, D. A.; Reches, M.; Whitesides, G. M. Low-Cost Printing of Poly(Dimethysiloxane) Barriers to Define Microchannels in Paper. *Anal. Chem.* **2008**, *80*, 3387−3392.
(19) Määttänen, A.; Fors, D.; Wang, S.; Valtakari, D.; Ihalainen, P.; Peltonen, J. Paper-Based Planar Reaction Arrays for Printed Diagnostics. *Sens. Actuators, B* **2011**, *160*, 1404−1412.
(20) Chitnis, G.; Ding, Z.; Chang, C.; Savran, C.; Ziaie, B. Laser Treated Hydrophobic Paper: An Inexpensive Microfluidic Platform. *Lab Chip* **2011**, *11*, 1161−1165.
(21) Carrilho, E.; Martinez, A. W.; Whitesides, G. M. Understanding Wax Printing: A Simple Micropatterning Process for Paper Based Microfluidics. *Anal. Chem.* **2009**, *81*, 7091−7095.
(22) Lu, Y.; Shi, W.; Jiang, L.; Qin, J.; Lin, B. Rapid Prototyping of Paper-Based Microfluidics with Wax for Low-Cost, Portable Bioassay. *Electrophoresis* **2009**, *30*, 1497−1500.
(23) Lu, Y.; Shi, W.; Qin, J.; Lin, B. Fabrication and Characterization of Paper-Based Microfluidics Prepared in Nitrocellulose Membrane by Wax Printing. *Anal. Chem.* **2010**, *82*, 329−335.
(24) Dungchai, W.; Chailapakul, O.; Henry, C. S. A Low-Cost, Simple and Rapid Fabrication for Paper-Based using Wax Screen Printing. *Analyst* **2011**, *136*, 77−82.
(25) Songjaroen, T.; Dungchai, W.; Chailapakul, O.; Laiwattanapaisal, W. Novel, Simple and Low-Cost Alternative Method for Fabrication of Paper-Based Microfluidics by Wax Dipping. *Talanta* **2011**, *85*, 2587−2593.
(26) Liana, D. D.; Raguse, B.; Justin Gooding, J.; Chow, E. Recent Advances in Paper-Based Sensors. *Sensors* **2012**, *12*, 11505−11526.
(27) Yetisen, A. K.; Akram, M. S.; Lowe, C. Paper-Based Microfluidic Point-of-Care Diagnostic Devices. *Lab Chip* **2013**, *13*, 2210−2251.
(28) Santhiago, M.; Nery, E. W.; Santos, G. P.; Kubota, L. T. Microfluidic Paper-Based Devices for Bioanalytical Applications. *Bioanalysis* **2014**, *6*, 89−106.
(29) Balu, B.; Berry, A. D.; Wess, D. H.; Breedveld, V. Patterning of Superhydrophobic Paper to Control the Mobility of Micro-Liter Drops for Two-Dimensional Lab-on-Paper Applications. *Lab Chip* **2009**, *9*, 3066−3075.
(30) Barona, D.; Amirfazli, A. Producing a Superhydrophobic Paper and Altering its Repellency through Ink-jet Printing. *Lab Chip* **2011**, *11*, 936−940.
(31) Stepien, M.; Saarinen, J. J.; Teisala, H.; Tuominen, M.; Aromaa, M.; Kuusipalo, J.; Mäkelä, J. M.; Toivakka, M. Surface Chemical Characterization of Nanoparticle Coated Paperboard. *Appl. Surf. Sci.* **2012**, *258*, 3119−3125.
(32) Stepien, M.; Saarinen, J. J.; Teisala, H.; Tuominen, M.; Aromaa, M.; Haapanen, J.; Kuusipalo, J.; Mäkelä, J. M.; Toivakka, M. ToF-SIMS Analysis of UV-Switchable TiO_2 Nanoparticle Coated Paper Surface. *Langmuir* **2013**, *29*, 3780−3790.
(33) Mäkelä, J. M.; Aromaa, M.; Teisala, H.; Tuominen, M.; Stepien, M.; Saarinen, J. J.; Toivakka, M.; Kuusipalo, J. Nanoparticle Deposition from Liquid Flame Spray onto Moving Roll-to-Roll Paperboard Material. *Aerosol Sci. Technol.* **2011**, *45*, 827−837.
(34) Teisala, H.; Tuominen, M.; Aromaa, M.; Mäkelä, J. M.; Stepien, M.; Saarinen, J. J.; Toivakka, M.; Kuusipalo, J. Development of Superhydrophobic Coating Paperboard Surface Using the Liquid Flame Spray. *Surf. Coat. Technol.* **2010**, *205*, 436−445.
(35) Abramoff, M. D.; Magalhaes, P. J.; Ram, S. J. Image Processing with Image. *J. Biophotonics* **2004**, *11*, 36−42.
(36) Teisala, H.; Tuominen, M.; Stepien, M.; Haapanen, J.; Mäkelä, J. M.; Saarinen, J. J.; Toivakka, M.; Kuusipalo, J. Wettability Conversion on the Liquid Flame Spray Generated Superhydrophobic TiO_2 Nanoparticle Coating on Paper and Board by Photocatalytic Decomposition of Spontaneously Accumulated Carbonaceous Overlayer. *Cellulose* **2013**, *20*, 391−408.
(37) Hashimoto, K.; Irie, H.; Fujishima, A. TiO_2 Photocatalysis: A Historical Overview and Future Prospects. *Jpn. J. Appl. Phys.* **2005**, *44*, 8269−8285.
(38) Tatsuma, T.; Kubo, W.; Fujishima, A. Patterning of Solid Surfaces by Photocatalytic Lithography based on the Remote Oxidation Effect of TiO_2. *Langmuir* **2002**, *18*, 9632−9634.
(39) Tuominen, M.; Teisala, H.; Haapanen, J.; Aromaa, M.; Mäkelä, J. M.; Stepien, M.; Saarinen, J. J.; Toivakka, M.; Kuusipalo, J. Adjustable Wetting of Liquid Flame Spray (LFS) TiO_2-Nanoparticle Coated Board: Batch-type versus Roll-to-Roll Stimulation Methods. *Nord. Pulp Pap. Res. J.* **2014**, *29*, 271−279.
(40) Extrand, C. W. Spontaneous Spreading of Viscous Liquid Drops. *J. Colloid Interface Sci.* **1993**, *157*, 72−76.
(41) Washburn, E. W. The Dynamics of Capillary Flow. *Phys. Rev.* **1921**, *17*, 273−283.
(42) Rye, R. R.; Man, J. A., Jr; Yost, F. G. The Flow of Liquids in Surface Grooves. *Langmuir* **1996**, *12*, 555−565.
(43) Rosina, J.; Kvasnák, E.; Suta, D.; Kolárová, H.; Málek, J.; Krajci, L. Temperature Dependence of Blood Surface Tension. *Physiol. Res.* **2007**, *56*, 93−98.
(44) Merrill, E. W. Rheology of Blood. *Physiol. Rev.* **1969**, *49*, 863−888.
(45) Shukla, P. C.; Chaube, D. K. Comparative Studies on Physical Properties of Urine and Urine-Oxalic Acid Mixture of Healthy Individual and Patients Suffering from Urinary Calculi. *Asian J. Chem.* **1996**, *8*, 22−30.